#### Peer-reviewed Statement

# Climate Extremes at the City–River Interface: Insights from the Philadelphia-Schuylkill System

By Dingyu Xuan, M. Ani Hsieh, Leandro S. Pongeluppe, Mackenzie M. Weaver, Michael E. Mann, Douglas Jerolmack & Hugo N. Ulloa.

This is a non-reviewed preprint submitted to EarthArXiv. Subsequent versions may have slightly different content after peer review.

# Climate Extremes at the City–River Interface: Insights from the Philadelphia-Schuylkill System

D. Xuan<sup>1,2</sup>\*, M. A. Hsieh<sup>3,4</sup>, L.S. Pongeluppe<sup>5</sup>, M. M. Weaver<sup>1</sup>, M. E. Mann<sup>1</sup>, D. J. Jerolmack<sup>1,4</sup>, and H. N. Ulloa<sup>1</sup>\*

Hurricane Ida struck the U.S. East Coast in August 2021, pushing the Schuylkill River in Philadelphia to a record discharge nearly 100 times larger than its average flow. As one of the most severe disasters of the 21st century, Ida exemplifies the increasing frequency and intensity of extreme hydrometeorological events under climate change. Predicting urban flood pathways remains challenging due to the complex interplay of rainfall-runoff and river–tide–landscape interactions. To address this, we developed a high-resolution (street-resolved) flood model integrating Li-DAR terrain data, bathymetric surveys, and land use-based surface friction across Philadelphia. We find that impervious surfaces and fragmented infrastructure exacerbate pluvial flooding and localized waterlogging, increasing exposure for both low- and high-income communities. Scenario-based simulations reveal a tipping point: a logarithmic increase in inunda-

10

11

12

13

14

15

16

<sup>&</sup>lt;sup>1</sup> Department of Earth and Environmental Science, University of Pennsylvania, USA

<sup>&</sup>lt;sup>2</sup> Department of Civil and Environmental Engineering, Imperial College London, UK

<sup>&</sup>lt;sup>3</sup> Department of Computer and Information Science, University of Pennsylvania, USA

Department of Mechanical Engineering and Applied Mechanics, University of Pennsylvania, USA
<sup>5</sup> Wharton School, University of Pennsylvania, USA

<sup>\*</sup>To whom correspondence should be addressed; E-mail: dyxuan@sas.upenn.edu, ulloa@sas.upenn.edu

tion areas for return periods above 100 years, and 2-7% additional flooding when peak discharge coincides with high tide—rising to up to 15% under projected sea level rise by 2100. Our findings underscore the compounding impacts of climate extremes in urban river systems and the need for integrated forecasting and adaptive planning—particularly in vulnerable, low-lying, and rapidly urbanizing regions worldwide.

# **Introduction**

17

20

21

22

Hurricane Ida made landfall as a Category 4 hurricane in Louisiana on August 29, 2021, unleashing strong winds, storm surges, and intense rainfall that devastated the Gulf Coast 1,2. As it moved inland, remnants of the storm and seven tornadoes that struck Philadelphia between September 1-2 triggered an unprecedented discharge and a 1-in-100-year flood along the Schuylkill River, causing widespread damage<sup>3</sup>. Extreme hydrometeorological events (EHMEs) like Ida have caused average global losses of \$136.7 billion annually (2003-2022)<sup>4;5</sup>, surging to over \$350 billion in 2024 alone<sup>6</sup>. Rain-driven floods are expected to intensify with climate extremes and expanding urbanization, which constrains rivers and alters floodplain dynamics<sup>7;8;9;10</sup>. In tidally influenced rivers, sea-level rise (SLR) and stronger tropical cyclones further amplify flood severity and human vulnerability 11;12;13;14. Currently, 13.3% of the U.S. population—over 40 million people—is exposed to 1-in-100-year floods 15. However, future flood risks in urban and coastal areas remain poorly quantified 16;17;18;19, hindering effective mitigation 15;20. Philadelphia exemplifies this challenge: as the third-most populous east coast city in the U.S. (1.5M residents), it is bounded by the Delaware River to the east and bisected by the Lower Schuylkill River (Fig. 1A-C).

The Schuylkill River rushes through bedrock rapids as it enters Philadelphia, transi-

tioning from piedmont to coastal plain, where urban development is concentrated 21. Historically, the Schuylkill functioned as both sewer and navigation routes during the 19th century, supporting Philadelphia's rapid industrial and population growth<sup>22</sup>. By the 20th century, flood-control measures—channelization and levee construction—were introduced to reduce mounting flood risks<sup>23</sup>, such as Fairmount Dam. These interventions enabled dense riverside development but also severed the river's connection to its natural floodplain, diminishing its ability to absorb and regulate extreme events. Meanwhile, average annual discharge of the river (25-160 m<sup>3</sup>/s) has increased since 1931, typically peaking in spring but now showing more frequent and extreme autumn peaks from hurricane intensification under climate change <sup>24;25;26</sup>. Current infrastructure struggles with intensifying EHMEs, as demonstrated by Hurricane Ida. A broader knowledge gap persists in understanding how urban rivers, especially those tidally influenced, respond to compounding stressors like EHMEs and SLR. This challenge extends far beyond Philadelphia, affecting cities worldwide where fluvial-tidal interactions remain poorly understood but can amplify flood impacts <sup>27;28;29;30;31</sup>. While hydrodynamic models hold promise for urban flood forecasting and resilience planning, several challenges remain: limited availability of detailed terrain data, sparse observations for model calibration, difficulties in integrating heterogeneous datasets, and trade-offs between computational efficiency and storage for fine-scale simulations 32;33;34;35.

Here, we develop a high-resolution flood modeling framework for the Philadelphia-Schuylkill system, employing the GPU-accelerated LISFLOOD-FP numerical framework <sup>36;37;38;39;40</sup>, to resolve street-level inundation dynamics. Our findings reveal a dual amplification of flood risk driven by urbanization: impervious surfaces increase runoff by reducing infiltration, while engineered infrastructure forms drainage bottlenecks that impede flow toward major waterways. We also identify Hurricane Ida's disproportionate impact on both low- and

high-income populations, who experienced comparable flood exposure—underscoring the need for targeted protection of vulnerable communities. We find that the Schuylkill River's current 100-year flood capacity ( $Q_{100} \approx 3,480 \text{ m}^3/\text{s}$ ) represents a tipping point: surpassing it triggers nonlinear increases in inundation extent. Additionally, climate change has compressed return periods—flows once considered 1-in-50-year events (e.g., 2,000 m $^3/\text{s}$  in the 1950s) now occur statistically every three years. Rainfall and topography primarily govern flood patterns, whereas tidally modulated downstream water levels can further expand inundation in riparian areas. While these findings provide critical guidance for urban planners and policymakers in Philadelphia, the challenges we uncover and tackle are in fact representative of riverine and coastal cities globally  $^{41}$ , each influenced by their own distinct environmental and socio-economic contexts.

#### **Results**

#### 78 Modeling framework

Our model integrates the city's first 5-m LiDAR-derived terrain model and the latest Schuylkill
River bathymetry survey to best calculate flow direction. Surface roughness is then calibrated from National Land Cover Datasets based on the relationship between frictional
Manning coefficients and land use (*Materials and Methods*). The model solves the interaction of upstream river flow, downstream tidal elevation, and rainfall across the domain,
as three primary boundary conditions. The outputs include water depth, flow velocity and
discharge.

To validate the model's ability to reproduce flooded areas within the floodplain, we used citizen-reported data, drone and satellite images, and on-site observations<sup>42</sup>. Drone images from Hurricane Ida closely match the model's outputs, especially along the east bank

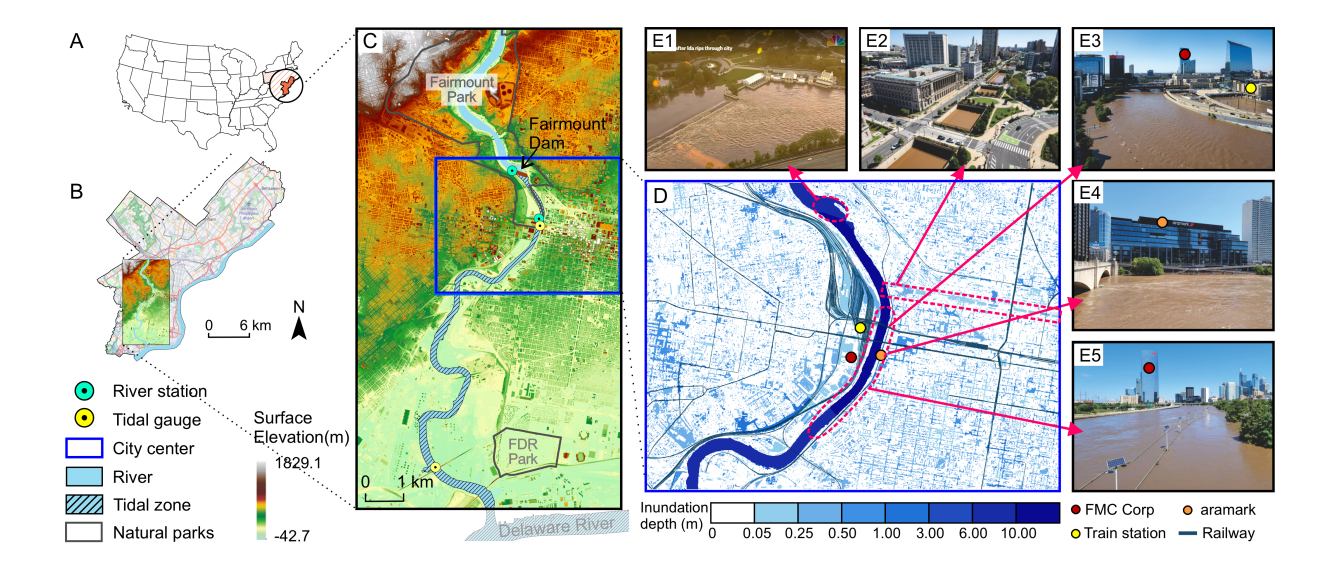


Figure 1: Map of research area and flood inundation of the Center City validated by drone images. (A) The location of Philadelphia in the US. (B) Research area in Philadelphia overlaid with Open Street Map. (C) Surface elevation of the study area. (D) Flood inundation map based on the Digitial Surface Model (DSM) with railway lines overlaid. (E1 - E5) Drone images with identifiable landmarks were collected from social media, illustrating the actual inundated areas: (E1) the area in front of the Fountain of the Sea Horses near the Philadelphia Museum of Art<sup>42</sup>; (E2) Vine Street Expressway; (E3) Amtrak rail yards; (E4) in front of the Aramark Global Headquarters; (E5) the Schuylkill Boardwalk, which is nearly submerged; (E2 - E5 were sourced from online media 43 and photographed by Mark Henninger).

of the Schuylkill River near Center City. The model effectively reproduce severe flooding in Fairmount Park, near the Philadelphia Museum of Art, Vine Street, and the Schuylkill Trail (Fig. 1D-E). We estimated flood extent and magnitude using satellite imagery and hydrodynamic *in situ* measurements (*Materials and Methods*), finding that the model reproduces 68% of flooded areas in urban areas and over 90% of river discharge and water level along the channel.

#### Uncovering Ida flood footprint in Philadelphia

104

108

109

111

112

Like many cities built along tidally influenced rivers, Philadelphia's flood severity is shaped by three key factors: watershed rainfall, river discharge, and tidal surges. The Fairmount Dam marks the upstream tidal limit of the Schuylkill River (Fig. 1C). Downstream, the tidally affected reach flows between Center City to the east and major hospitals and universities to the west, flanked by dense transportation infrastructure (Fig. 1D). Our analysis reveals that the east bank is particularly vulnerable to flooding due to its lower elevation, direct 101 connectivity to roadways and tunnels, and localized erosion. This risk is most pronounced in the central region of the Lower Schuylkill (Fig. 1D). 103

Flooding also significantly impacted transportation infrastructure. Nearly all railway adjacent to the river experienced disruption: east bank lines, situated closer to the channel, were primarily affected by overbank flow, while west bank lines were more susceptible to intense rainfall (Fig. 1E3-5). The convergence of fluvial and pluvial drivers created a substantial hazard, particularly along the east bank, with floodwaters extending into the urban core.

But why was Hurricane Ida's impact in Philadelphia so severe? Extensive impervious 110 surfaces and pre-saturated soils likely intensified surface runoff, increasing river discharge. These conditions highlight the role of urbanization and antecedent hydrometeorological states in amplifying flood severity during extreme events.

# **Urbanization and Prior Hydrometeorology Shaping Flood Risk**

To examine the role of urbanization in the flood severity, we conducted numerical simulations of the Lower Schuylkill River during Hurricane Ida (September 1-3, 2021) using two digital elevation models: a bare-earth Digital Terrain Model (DTM) and an infrastructureinclusive Digital Surface Model (DSM) (Fig. 2A-B). The DTM-based simulation reveals more extensive riverine flooding, with surface runoff naturally concentrating along topographic lows and channel networks. In contrast, the DSM simulation—incorporating buildings, roads, and levees—exhibits less overbank flooding but broader distributed inundation across the urban landscape.

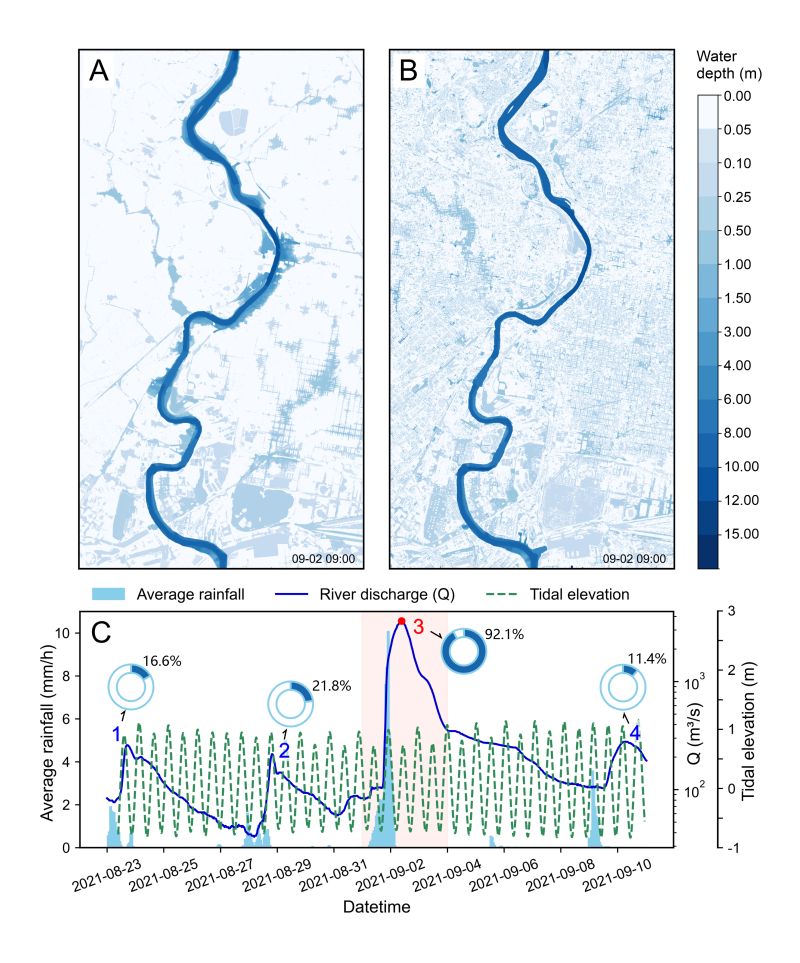


Figure 2: Inundation map resulting from Hurricane Ida using different elevation models. Flood inundation based on DTM (A) and DSM (B) at 9 a.m. on September 2, 2021, shown as the red point in (C). (C) Time series of average rainfall for the whole upstream watershed, river discharge at the upstream boundary condition, and tidal elevation at the downstream boundary condition. The numbers along the discharge line correspond to four distinct peaks in river discharge, with the adjacent doughnut charts illustrating the respective runoff coefficients. Each complete doughnut chart represents the cumulative rainfall leading up to each peak, while the blue-shaded portion depicts the proportion of that rainfall converted into surface runoff. The light orange-shaded area marks the occurrence of the extreme event, which took place between September 1 and September 3, 2021.

This spatial pattern reflects two key effects of urbanization. First, engineered riverbanks 123 and levees constrain lower-Return-Period floods, reducing overtopping and limiting floodplain spread. Second, impervious surfaces and built structures impede drainage, trapping water in depressions and generating localized, stagnant flooding. These shallow inundations disproportionately affect pedestrian and vehicular mobility in low-lying urban neighborhoods. Overall, the DSM scenario (Fig. 2B) results in a 30% increase in inundated area and an approximately 8% increase in downstream river peak compared to the DTM (Fig. 2A), underscoring the compound influence of urban form and topography on flood hazards in cities like Philadelphia.

125

126

127

128

129

130

131

147

In addition to reduced infiltration caused by urbanization, antecedent soil moisture criti-132 cally influences flood severity during EHMEs. Prior to Hurricane Ida, two moderate storms 133 (events 1 and 2 in Fig. 2C) progressively saturated the watershed. We assessed infiltration-134 runoff dynamics using the runoff coefficient ( $\mathcal{C}$ ), defined as the fraction of precipitation con-135 verted to surface runoff. Four discharge peaks were analyzed: "peaks 1" and "2" before Ida, 136 "peak 3" during the main flood, and "peak 4" after recession. Although rainfall before "peak 137 2" was lighter than before "peak 1", it generated more runoff, indicating that the four-day dry interval was insufficient for soil to recover infiltration capacity. This suggests that soils were already near saturation three days before Ida. Consequently, nearly all rainfall during the main event was converted to runoff. While cumulative rainfall before "peak 3" was only 5.5 times that of "peak 2", river discharge was 23.2 times greater, corresponding to a peak  $\mathcal C$  of 92.1%. One week later,  $\mathcal{C}$  dropped below 12.0%, signaling a return to baseline hydrologic conditions. These findings highlight the critical role of antecedent hydrologic conditions in shaping EHME-induced flooding. Ignoring pre-event soil moisture can lead to substantial 145 underestimation of runoff and flood severity in urban flood models. 146

The strong influence of both urban form and hydrologic state on inundation patterns

raises a pressing question for climate adaptation: Who is most at risk during extreme
weather events? This concern is especially acute in densely populated cities with socioeconomic disparities and aging infrastructure, where compound flooding can exacerbate
vulnerabilities and amplify inequities.

#### Flood Inequality and Economic Impacts in Philadelphia

We quantified individual-level flood risk using a Socioeconomic Vulnerability Index (SEVI)
that averages eight indicators—housing burden, language, educational attainment, age,
race, employment status, and poverty—following <sup>44</sup> (Fig. 3A; *Materials and Methods*). The
SEVI serves as a proxy for socioeconomic status and stratifies residents into five groups.
Across groups, housing burden, low educational attainment, and racial discrimination contribute most, whereas age contributes least in this study site.

Our analysis reveals that both the lowest and highest SEVI groups are disproportion-159 ately vulnerable to flooding. Despite accounting for relatively small shares of the total inundated area, these groups exhibit the highest rates of population exposure—over 20% in both 161 cases (Fig. 3B). For high-SEVI communities, heightened exposure likely stems from insuffi-162 cient flood preparedness and systemic neglect of environmental protections 45. In contrast, 163 low-SEVI populations, face increased flood risk due to extensive impervious surfaces and localized land subsidence—measured at 1-3 mm per year—driven by groundwater with-165 drawal and compaction from dense infrastructure 46;47;48. While proximity to water bodies 166 offers low-SEVI residents recreational and aesthetic benefits, it also amplifies their expo-167 sure to fluvial hazards. Moreover, flooding in these economic hubs, such as Center City, 168 can lead to substantial indirect losses, including business disruptions, and infrastructure 169 damage that delay post-disaster recovery. 170

In terms of total flood-affected area, the 40-60% SEVI group experienced the most

171

widespread inundation, reflecting that the majority of census tracts within this study site
fall in this socioeconomic vulnerability range in Philadelphia relative to Pennsylvania. Beyond these densely populated regions, urban green spaces such as Fairmount Park and
FDR Park serve a dual function: providing essential recreational and cultural access while
acting as natural hydrological buffers. These parks mitigate downstream flood impacts by
absorbing and temporarily storing stormwater. However, during sequences of moderate
rainfall followed by extreme events, their storage capacity may be exceeded, contributing to
elevated surface runoff and intensified flood severity.

To better assess the economic and financial damages caused by Hurricane Ida in 180 Philadelphia relative to other regions of Pennsylvania, we estimated the zipcode-level im-181 pact using U.S. Small Business Administration (SBA) disaster loan data <sup>49;50</sup>. This analysis 182 reveals a pronounced disparity in Ida's economic effects across Pennsylvania: on average, 183 verified losses were significantly higher in Philadelphia, USD 160,061 per zipcode, while 184 approved SBA disaster loans increased by only USD 13,997—a statistically non-significant 185 difference (Fig. 3D). These results indicate that, although Philadelphia sustained dispropor-186 tionately greater damage, monetary support did not scale with the magnitude of its losses. 187 The divergence between verified losses and loan disbursements points to structural limits in post-disaster financial mechanisms, particularly in dense urban areas where exposure and damage intensity are greatest.

These estimated impacts were further used to assess the disaster's financial implications <sup>51</sup>. Across a range of discount and default rate sensitivity scenarios, the resulting net present values (NPVs) remain consistently negative, ranging from USD 19.9 to USD 21.4 million. From a societal perspective, Hurricane Ida imposed a significant and persistent welfare loss on Philadelphia, only partially offset by existing governmental credit-based relief. Together, these findings underscore the disproportionate economic exposure of urban cen-

191

193

194

ters, such as Philadelphia, to climate extreme disasters and their limited financial resilience

even under dedicated federal assistance programs.

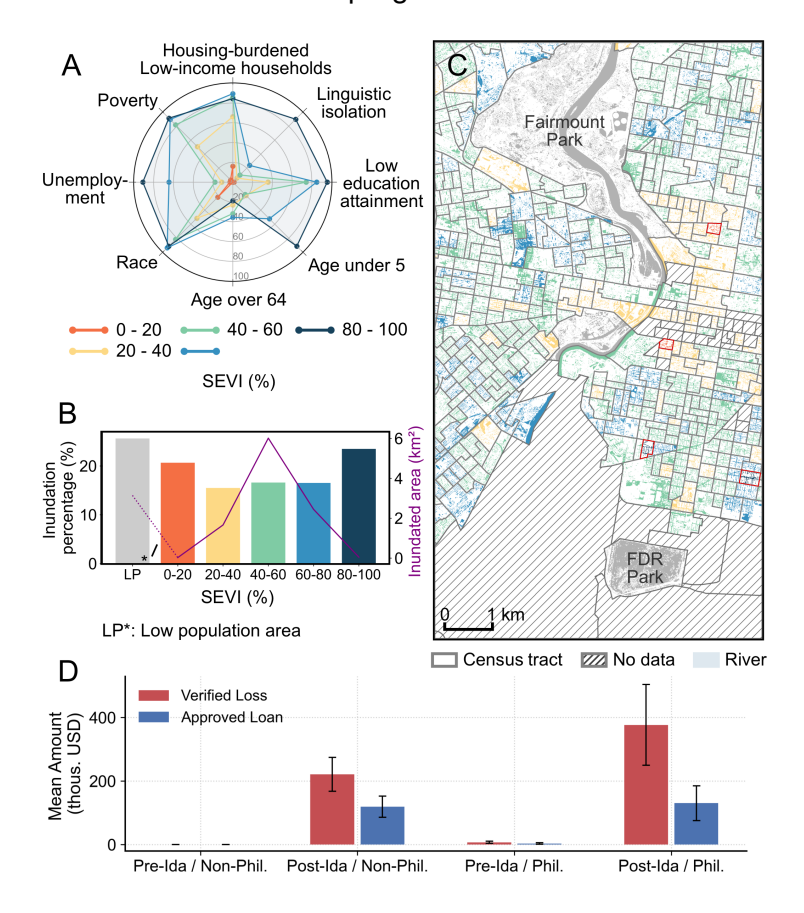


Figure 3: Effect of socioeconomic situation on flood inundation and economic consequences of this event. (A) Eight components of different socioeconomic vulnerability indices (SEVI) and their contributions in different SEVI groups. The values for each component represent the average values within each SEVI group (see *Materials and Methods*). Here, a higher SEVI indicates more impoverished socioeconomic situation. (B) Inundation percentages and areas of different SEVI groups for this 2021 flood event. SEVI groups exclude the census tract with a population density less than 10 people per square kilometer, shown as the gray region in panel C. (C) Inundation in regions with different SEVI. Different color indicates different SEVI groups shown in panel B. The most affected groups (0-20% and 80-100%) are highlighted with red boundaries. (D) Verified losses and approved loans in Pennsylvania Pre- and Post-Ida Hurricane. Data from Small Business Administration US at the zipcode-year level.

#### Outlook for Future Floods

#### Schuylkill in a changing climate

208

209

210

We analyzed return periods for the Schuylkill River over the past century (*Materials and Methods*) and identified the 2021 flood as the largest fluvial event on record. The relationship between discharge and return periods follows a logarithmic trend, which we used to extrapolate peak flows for more extreme events (Fig. 4A). A more detailed examination of annual peak flows reveals a sustained upward trend, particularly for high-return-period events.
Frequency analyses of successive 20-year periods confirm this intensification (Fig. 4B–C),
providing direct evidence of climate-driven extremes in the local hydrologic regime.

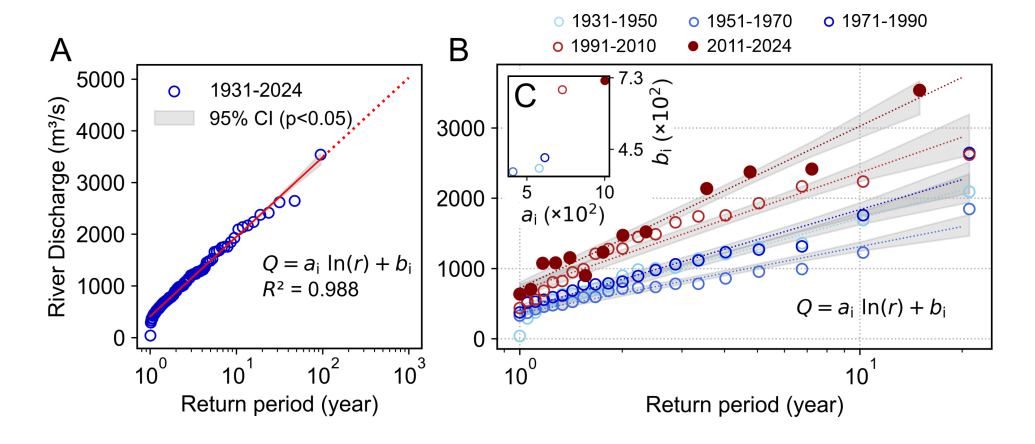


Figure 4: River discharge and flood inundation across different return periods. River discharge frequencies for the Schuylkill River are analyzed over the past century (A) and by every 20-year interval (B), with return periods estimated using the annual maxima series and the Weibull plotting position formula. Logarithmic trend line follows Q =  $a_i \ln(r) + b_i$ , with coefficients' values shown in panel (C); for the full period,  $a_0 = 667 \text{ m}^3/\text{s}$ ,  $b_0 = 416 \text{ m}^3/\text{s}$ . All fits yield  $R_i^2 > 0.93$ . Gray shaded areas indicate 95% confidence intervals.

To assess the implications of these trends, we simulated flood inundation across eight synthetic hydrographs, representing return periods from 5 to 5000 years. These were generated using the extrapolated discharge relationship  $Q = a_0 \ln(r) + b_0$  and a standardized hydrograph based on historical events. Six cross-sections—three upstream and three down-

stream of Fairmount Dam—were selected to evaluate spatial variations of the City-River interface in response to the flood (Fig. 5A). River levels rise predictably with increasing discharge, but a sharp inflection occurs near the 100-year threshold. Below this threshold, floodwaters are typically contained within engineered riverbanks; above it, inundation expands rapidly in a logarithmic fashion (Fig. 5B), revealing the nonlinear escalation of flood hazard.

This nonlinear behavior is tightly linked to local topography and human infrastructure. During events with return periods shorter than 100 years, floodwaters remain largely confined by steep channelized banks and auxiliary structures such as raised terraces and refuge islands. However, floods of higher return periods exceed the capacity of both primary

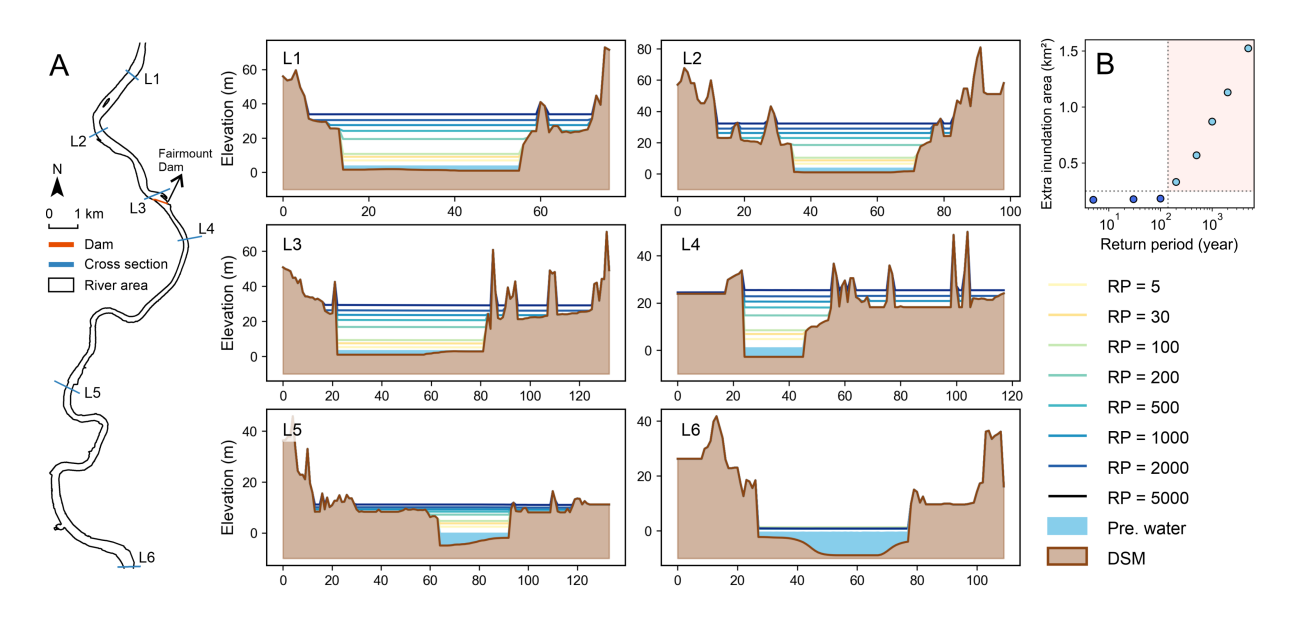


Figure 5: Cross sections and inundation extents of the Schuylkill River under different return periods (RP). (A) Top-down view of the Schuylkill River showing six selected cross sections near existing gauge stations. Three of these sections are situated upstream the of dam, while the remaining three are downstream. The "Pre. water" area represents the initial water level accumulated during the model's spin-up process. (B) River flood inundation extents for each RP, excluding the surface area of the Schuylkill River under pre-flood conditions. The light orange shaded area illustrates the logarithmic range of inundation growth, indicating that a critical flood threshold lies above the 100-year RP inflow.

and secondary defenses, inundating wider urban areas (Fig. 5A, panels L1–L6). Given the documented rise in extreme discharges (Fig. 4B–C), what is currently classified as a 100-year flood may become significantly more frequent. This evolving threat is compounded by tidal dynamics and sea level rise, which amplify overbank flooding and extend inundation into areas previously deemed low-risk.

#### Tides and Sea Level Rise (SLR)

The interaction between the flood wave triggered by Hurricane Ida and a low but rising tide (Fig. 2C, "peak 3") raises the question of how downstream surface water elevation  $\eta(t)$ —modulated by tides at short timescales and SLR over long timescales—influences flood extents along the Lower Schuylkill River.

To quantify tidal influences, we performed spectral analysis of  $\eta(t)$  over a two-year period, identifying dominant tidal constituents and their key properties: amplitude, phase, and period. Semi-diurnal tides emerged as the primary drivers of variability, producing daily fluctuations that shift with the 14.7-day spring—neap cycle. We also detected the annual King tide, which sets extreme tidal conditions downstream of Fairmount Dam. Because tidal stage and river discharge are statistically independent (*Materials and Methods*), we applied harmonic analysis to reconstruct tidal behavior and assess compound flood risk scenarios. We simulated worst-case flooding by combining the King tide with projected SLR trajectories.

Under projected SLR scenarios for 2040 and 2100<sup>52</sup>, a 100-year flood could inundate an additional 10,000 m<sup>2</sup> along the Schuylkill River, potentially affecting over 100 more city blocks (Fig. 6A). To quantify the effect of extreme tide conditions on fluvial flooding, we computed the difference of inundated areas driven by the highest and lowest tide amplitude over a year. This difference increases sharply for return periods between 100 and 1000 years

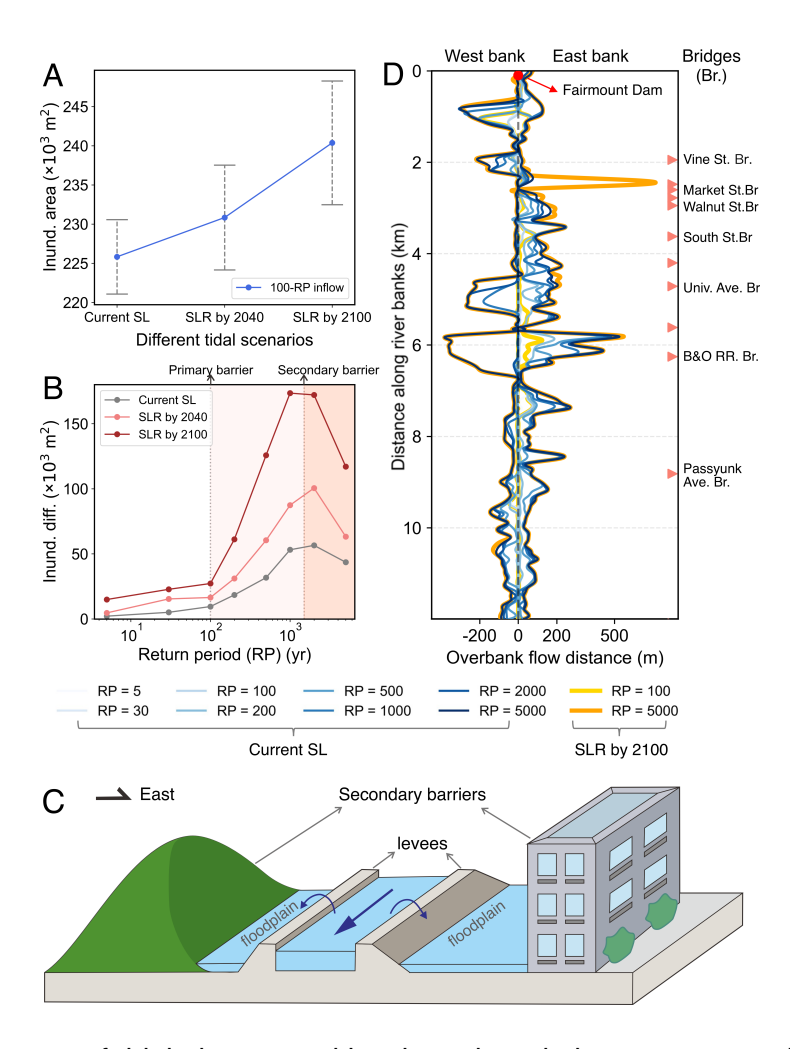


Figure 6: The impact of tidal phases and levels on inundation patterns and their combined effect with river discharge under different return periods (RP). (A) The scatter plot shows the average inundated area under 100-year RP river inflows, with dashed lines representing the range of inundation caused by extreme tides conditions, i.e., between the lowest and the King tide. In most cases, the largest inundated areas correspond to King tide conditions, and the lowest areas align with the lowest tide. Projected sea level rise (SLR) is based on localized estimates along the Delaware River, with increases of 0.5 meters by 2040 and 1.4 meters by 2100<sup>52</sup>. (B) Differences in inundated area between King tide and the lowest tide in 2021 are shown across various river inflow RPs. The King tide and the lowest tide were aligned with the river discharge peak in the corresponding hydrograph for each simulation. (C) Schematic diagram of the primary and secondary barriers. (D) Overbank flow distance for various RPs river flows within the tidally affected section of the river. Distance along the river (y-axis) is measured relative to the Farimount Dam. Bridge names on the right are used for positioning.

(Fig. 6B), primarily because the flood wave is less restricted after overtopping engineered levees and spreads through floodplains before reaching secondary barriers (Fig. 6C). On the west bank, natural terraces provide this secondary barrier, while on the east bank, a combination of built structures and elevated landforms—especially in the river's upper reach—play this role. Once floodwaters reach the second barriers, the floodplain becomes fully submerged, and additional tidal influence has limited effect, as indicated by the leveling off of inundated area beyond the 1000-year return period.

Overbank flow analysis along the tidally influenced reach (Fig. 6D) reveals consistently higher flood vulnerability on the east bank, corroborating both drone observations and model results from Hurricane Ida. The west bank on the other hand, especially between 2 and 4.2 km, remains comparatively protected. A critical high-risk zone emerges near 2.2 km on the east bank, between the Vine Street Corridor (Fig. 1E2) and Market Street Bridge, where SLR amplifies flood risk to underground transportation infrastructure. These findings underscore the spatial variability of tide-modulated flood hazards and highlight the importance of targeted, site-specific adaptation strategies along the Lower Schuylkill River.

# Changing Storm Characteristics

253

254

257

259

260

Past studies  $^{53}$  have demonstrated that projected changes in tropical cyclone storm surges add to sea level rise in increasing coastal risk along the U.S. mid-Atlantic coast. Using a tropical cyclone down-scaling method driven by large-scale climate model simulations, Garner et al  $^{53}$  found that increases in both hurricane intensity and hurricane size (as measured by radius of maximum wind) contribute to increased likelihood of very large storm surges with continued warming. They focused specifically on New York City's Battery Park and the likelihood of future Super storm Sandy-like inundation events, the return period of which is estimated to decrease from  $\sim$ 25 years today to  $\sim$ 5 years mid-century in a fossil fuel inten-

sive policy scenario. A similar analysis could be applied to the Schuylkill River catchment to assess the combined role of sea level change and changing storm characteristics in future projected coastal flooding risk for the Schuylkill watershed.

# **Discussion**

278

280

281

287

288

289

Hurricane Ida produced record flooding on the Schuylkill—a nominal 1-in-100-year event.

Century-scale records show such extremes are becoming more frequent and intense, with

peak flows shifting from spring snowmelt to late-summer, often tropical, storms. These

trends demand climate-informed risk assessment.

Urbanization and wet antecedent soils amplify floods: impervious cover curtails infiltration and fragments flow paths, producing localized pooling rather than the channelized flooding typical of rural basins <sup>54</sup>. As heavy-rain bands penetrate inland <sup>55</sup>, cities like Philadelphia face more fluvial flooding—even without local rain. In our simulations, leves and embankments contain moderate events while buildings act as secondary barriers; once flows exceed the 100-year level, inundation expands rapidly. Designed for stationary hydrology, these defenses underperform in a changing climate <sup>56</sup>. A ~30 mm storm (~ 2 mm/h) can take ~1 week to drain, so closely spaced storms saturate soils, boost runoff, and stress stormwater systems. Despite omitting subsurface drainage, the model reproduces Ida-driven flooding and identifies priority upgrade areas <sup>45</sup>.

Our modeling framework<sup>57</sup> integrates land use, urban infrastructure, rainfall, river discharge, and tides  $^{36;37;38;39;40}$ , but several gaps bound inference. Near-term upgrades include spatially variable infiltration, explicit subsurface drainage, and wind effects on river dynamics and surge  $^{35}$ . Evaporation was neglected given its small contribution ( $\sim$ 0.3% of basal discharge  $^{58}$ ). Morphology is static, though extreme flows can reshape channels  $^{59;60}$ . On the Schuylkill, suspended sediment concentration rises sharply once riverbed shear ex-

ceeds  $\sim$ 24 Pa (discharge > 100 m<sup>3</sup>/s); sediment records cover less than 10 years (1959-1968), underscoring monitoring gaps.

Given these bounds, compound controls remain decisive in the tidally influenced Lower 296 Schuylkill: risk spikes when river peaks coincide with high tide, and sea-level rise (SLR) amplifies this hazard. With  $\sim$ 1.4 m SLR by 2100, a 100-year flood could expand inundation 298 by up to 15%, with larger increases for rarer events. Flood extent and pathways reflect 299 hydrology and the built environment; mapping these constraints reveals hotspots and areas 300 where riverine risk shifts to rainfall-driven flooding. Neighborhoods > 500 m from the river 301 generally face lower fluvial exposure, though local topography and drainage still govern 302 residual risk. 303

Effective risk reduction requires geographically tailored strategies. The east bank's proximity to major roads and transit concentrates riverine exposure; the higher west bank's flatlands and rail yards are more prone to pluvial flooding. Both high- and low-income groups are exposed, but in different ways: higher-income riverfront and Central Business District can face elevated exposure from subsidence and infrastructure loading, while lowerincome communities may lack preparedness resources and experience prolonged recovery, including public-health risks from sewage contamination 61;62. Quantitative assessments of 310 long-term socio-economic impacts (displacement, unemployment, educational disruption, mental health) remain scarce<sup>45</sup>.

304

305

306

307

308

309

311

313

315

316

Despite data constraints — especially acute in under-resourced regions 63;33;64 — hydrodynamic models remain essential for resilience planning under evolving hydrometeorology. Rising peak discharges for a given return period and pervasive SLR argue for climateadaptive, not fixed-in-time, infrastructure to attenuate flood waves 65;66;67. Nature-based solutions (e.g., Fairmount Park and FDR Park as stormwater "sponges") can cost-effectively complement gray systems <sup>68;69;70</sup>. Expanding access to high-resolution topography, pre-

cipitation forecasts, and high-performance modeling enables robust, real-time flood forecasting to protect vulnerable populations and critical assets. Philadelphia's priorities are: (i) compound-aware standards for capital projects (joint rainfall-river-tide-SLR design events; 321 updated maps/codes); (ii) green-gray hybrids-floodable open space and expanded stor-322 age in Fairmount and FDR Parks—paired with hardened utilities and rail yards 68;69;70; (iii) 323 real-time forecasting using high-resolution topography and ensemble precipitation; and (iv) 324 equitable adaptation that directs investment where hazard intersects socioeconomic vul-325 nerability, and prioritizes critical services in frontline neighborhoods. Closing sediment, 326 morphology, and drainage data gaps will reduce model uncertainty and sharpen prioritiza-327 tion 65;66;67. 328

We present a general approach to map flood risk from climate extremes in urban riverine systems. Using the Philadelphia–Schuylkill system as an exemplar, we show that compound interactions among river discharge, tides/sea-level rise, and the built environment
recur across coastal cities, offering a transferable framework for site-specific, equitable
adaptation.

#### Materials and Methods

#### Multidimensional Data Collection

River discharge upstream of the Fairmount Dam, at station PA-0147500, is obtained from 336 the USGS water database (https://waterdata.usgs.gov/monitoring-location/01474500/). Tidal 337 elevation downstream is available from a National Oceanic and Atmospheric Administration 338 (NOAA) tide gauge (PA-8543925) (https://tidesandcurrents.noaa.gov/noaatidepredictions.html). 339 Hourly precipitation grids were provided directly by the Office of Hydrological Development, 340 NOAA. 1-meter Digital terrain model (DTM), named as 3D Elevation Program (3DEP), was 341 available from USGS TNM Service (https://apps.nationalmap.gov/downloader/). Newly released LiDAR point cloud data, used to generate Digital Surface Model (DSM), is avail-343 able from a Philadelphia LiDAR survey (https://geo.btaa.org/catalog/pasda-7154). River bathymetry data was collected from the latest Lower Schuylkill survey provided by the US Army Corps of Engineers Philadelphia (https://www.nap.usace.army.mil/Missions/Civil-Works/Surveys/Projects/). Surface landscape is available from National Land Cover Database (NLCD) 2021 (https://www.usgs.gov/centers/eros/science/national-land-cover-database). Census tracts 2020, the boundary files of districts and watersheds in Philadelphia can be 349 downloaded from Open Data PHLmaps (https://data-phl.opendata.arcgis.com/datasets/). 350 Demographic data on census-tract level is available from 2017-2021 American Commu-351 nity Survey 5-Year Estimates on U.S. Census Bureau (https://data.census.gov/table/). The 352 latest Environmental justice dataset can be downloaded from PA Department of Environ-353 mental Protection (https://gis.dep.pa.gov/PennEnviroScreen/). U.S. Small Business Ad-354 ministration (SBA) dataset loss and loan datasets from 2000 to 2022 are available at 355 https://data.sba.gov/en/dataset/disaster-loan-data. The OpenFEMA dataset of disaster declarations summaries can be downloaded from the official website of the U.S. Department

of Homeland Security at https://www.fema.gov/openfema-data-page/disaster-declarationssummaries-v2. The Sentinel-2 satellite image is available from Copernicus Browser (https://browser.dataspa
The road network dataset is available from U.S. Census Bureau, Department of Commerce
(https://catalog.data.gov/dataset/).

#### LISFLOOD-FP Model Description

LISFLOOD-FP numerical solver is a 1D-2D raster-based hydrodynamic model based on the shallow water equations <sup>57</sup>, which enable the modeling of spatially and temporally varying processes like precipitation and local water discharges; it can be directly downloaded from Zenodo (https://zenodo.org/records/6912932). Here, we used the state-of-the-art acceleration hydrodynamic solver LISFLOOD-ACC <sup>57</sup> as a local inertial scheme to numerically resolve the water flow throughout a uniform grid describing the urban landscape, the floodplain, and the river channel e.g., <sup>71;72</sup>. This solver has been shown to have high fitting accuracy with real inundations and runs with NVIDIA GPU cores to significantly enhance the computational efficiency <sup>57</sup>.

# Watershed landscape and friction

The hydraulic resistance encountered by the river flow due to the land surface characteristics and the riverbed's composition is quantified by Manning's frictional coefficient (n). This
coefficient exhibits spatial variability and undergoes minor temporal changes. To establish
the spatial distribution of the Manning coefficient within our study area, we have leveraged
the United States Geological Survey (USGS) National Land Cover Dataset to analyze the
current land use following <sup>73;74</sup>. The determined Manning coefficient ranges from 0.027 to
0.160. This detailed mapping of the landscape friction allows capturing the subtle variability
in hydraulic resistance across the urban watershed of the Lower Schuylkill River.

# River Discharge Analysis

We conducted the frequency analysis to define return periods of the Schuylkill River by analyzing historical peak discharge from 1931 to 2024. The data before 1990 used the peak of daily average discharge due to the lower temporal resolution during that period, resulting in a slight smoothing of the peak values. Data from 1991 onward utilized peak flow values derived from 30-minute interval measurements. When comparing peak flows over consecutive 20-year periods, the return period was recalculated, as its value is correlated with the length of the dataset.

We used long-time series of river discharges to analyze the single-peaked hydrograph of the Schuylkill River and further design flood hydrographs of more severe river scenarios. The time when the river flow peaks is defined as the origin, with time values before and after negative and positive, respectively. The river discharge was scaled to 0 to 1 based on its proportion in the peak flow. The shape of a single-peaked hydrograph of the Schuylkill River is generally similar, so we assumed self-similarity in extrapolating flood waves to higher return periods. Rainfall intensities and associated river flows tend to follow the Gamma distribution flows, so exponential functions are used to model the withdrawal of flows flows flows, so exponential functions are used to model the withdrawal of flows flows, were used to fit the shape of the hydrograph. The hydrograph for a higher return period is designed by multiplying the fitted function by the calculated peak flow for a given return period based on the "similar-shape" assumption.

# Tidal Analysis

We used the Lomb-Scargle Periodogram Analysis, a spectral-density analysis method that is suitable for unequally spaced datasets, to detect the frequency of periodic signals of the

Schuylkill River within the latest two years of tidal elevation data<sup>78</sup>. Our results showed that the Schuylkill River is dominantly tidally modulated by the Lunar  $(M_2)$  and the Solar  $(S_2)$  semidiurnal tides, and  $K_1$  and  $O_1$  diurnal tide. Thus, we used four Fourier modes to fit and model the tidal elevation signal as a function of time:

$$\eta(t) = \eta_0 + \sum_{i=1}^4 A_i \sin \left[ 2\pi \frac{(t+t_0)}{T_i} + \varphi_i \right],$$
(1a)

$$t_0 = T_0 (TP_i - TP_0),$$
 (1b)

where  $\eta_0=0.074$  m.  $A_i$ ,  $T_i$ , and  $\phi_i$  are the amplitude, period, and phase of each tidal constituent.  $t_0$  is 0 in the real flood case, yet it varies based on different TPs. TP $_i$  represents a different tidal phase, while TP $_0$ , equal to 0.42, is the phase during the real event.  $T_0$  in Eq. 1b is a constant representing the semidiurnal period, approximately equal to 0.5 days.

To assess the relationship between river peak discharge and tidal levels, we computed Spearman and Kendall rank correlation coefficients. Both values indicate statical significance (Spearman = -0.124, p = 0.009; Kendall = -0.086, p = 0.007), yet their low magnitudes (|r| < 0.13) suggest a negligible association. Thus, the two variables can be considered approximately independent for modeling purposes.

# Socioeconomic Vulnerability Index (SEVI)

409

The SEVI is the average value of eight socioeconomic components, which are percentile values calculated for each census tract based on the distribution of all values across Pennsylvania 44. We excluded low-population-density areas when analyzing inundation for different SEVI groups to avoid misleadingly favorable Socioeconomic conditions. The value of the inundation percentage was calculated by dividing the total inundation area in each SEVI group by the total census tract areas in the same SEVI group.

The socioeconomic statistics were analyzed based on the 2010 census block groups rather than the latest 2020 groups to ensure consistency, as specific components still rely on the 2010 census geometries <sup>44</sup>. However, since the latest demographic data is based on 2020 census block groups, we assumed that the population density within the same census tract remains consistent regardless of location. We then recalculated the population density for these mismatched groups based on their respective area portions. This estimation had minimal impact on detecting low-population areas.

#### Model Validation

443

444

446

The model was challenged and well-validated through three methods. First, the overall inundation was qualitatively compared with one Sentinel-2 image, which was the only satellite
product with an acceptable cloud cover during this flooding event. We used the water indices AWEIsh<sup>79</sup> to extract the inundation area and set a 15-cm water depth threshold to
consider a wet cell<sup>80</sup> and quantify the inundation area. The "Hit rate" for the DTM and DSM
modeling results is 0.51 and 0.68, respectively, indicating positive correspondence. This
suggests the model adeptly captures the river channel expansion, even though there is a
tendency to overpredict the flood severity, particularly in urban areas. This overprediction
aligns with expectations since the model excludes infiltration and drainage networks.

Second, we used the model skill metric (MSM) to assess the modeling performance of the river discharge and surface elevation<sup>81</sup>. The MSMs' results consistently exceed 90%, affirming the model's exceptional ability to reproduce river hydrodynamics accurately.

Last, we used drone images with landmarks to compare the actual inundation extent with the model's predictions. This analysis revealed a strong alignment between the observed and modeled inundation areas, indicating the model's accuracy in representing real-world conditions.

# Data, Materials, and Software Availability

All data and codes are available at 10.5281/zenodo.1705541582 to reproduce our results.

# **Acknowledgments**

We greatly acknowledge the support from: the U.S. Army Corps of Engineers Philadelphia District for facilitating the latest sounding survey of the Schuylkill River, the National
Weather Service Middle Atlantic River Forecast Center for providing hourly precipitation
grids combining rain gauges with radar data, and the support of University of Pennsylvania's University Research Foundation (URF) Award. L.S.P. gratefully acknowledges support
from Leonard J. Horwitz, the Wharton Impact, and the Wharton AI & Analytics Initiative.

# **Author Declaration**

The authors declare no competing interests.

#### References

- Yi-Jie Zhu, Jennifer M Collins, Philip J Klotzbach, and Carl J Schreck III. Hurricane
   ida (2021): rapid intensification followed by slow inland decay. *Bulletin of the American Meteorological Society*, 103(10):E2354–E2369, 2022.
- 2. J. L. Beven, A. Hagen, and R. Berg. Tropical cyclone report: Hurricane ida, 2022.
- 3. Maria Pulcinella, Katie Meyer, and Kenny Cooper. Long recovery ahead as ida's remnants lead to historic flooding, tornadoes in philly region, 2021. Accessed: 2021-09-02.
- Frances V Davenport, Marshall Burke, and Noah S Diffenbaugh. Contribution of histor ical precipitation change to US flood damages. *Proceedings of the National Academy* of Sciences, 118(4):e2017524118, 2021.
- 5. CRED. 2023 disasters in numbers: A significant year of disaster impact. https://files.emdat.be/reports/2023\_EMDAT\_report.pdf, 2024. Accessed: 2024-04-05.
- 6. National Centers for Environmental Information (NOAA). Billion-dollar weather and climate disasters, 2024. Updated: 2024-11-01.
- 7. Hoesung Lee, Katherine Calvin, Dipak Dasgupta, Gerhard Krinner, Aditi Mukherji, Peter Thorne, Christopher Trisos, José Romero, Paulina Aldunce, Ko Barrett, et al. Climate change 2023: synthesis report. Contribution of working groups I, II and III to the sixth assessment report of the intergovernmental panel on climate change. 2023.
- 8. James D Miller and Michael Hutchins. The impacts of urbanisation and climate change on urban flooding and urban water quality: A review of the evidence concerning the United Kingdom. *Journal of Hydrology: Regional Studies*, 12:345–362, 2017.

- 9. Wei Zhang, Gabriele Villarini, Gabriel A Vecchi, and James A Smith. Urbanization
   exacerbated the rainfall and flooding caused by hurricane Harvey in Houston. *Nature*,
   563(7731):384–388, 2018.
- 10. A Rajib, Q Zheng, CR Lane, HE Golden, JR Christensen, II Isibor, and K Johnson.

  Human alterations of the global floodplains 1992–2019, sci. data, 10, 1–13, 2023.
- 11. S Wang and R Toumi. More tropical cyclones are striking coasts with major intensities at landfall. *Scientific reports*, 12(1):5236, 2022.
- 12. Renzhi Jing, Sam Heft-Neal, Daniel R Chavas, Max Griswold, Zetianyu Wang,
   Aaron Clark-Ginsberg, Debarati Guha-Sapir, Eran Bendavid, and Zachary Wagner.
   Global population profile of tropical cyclone exposure from 2002 to 2019. *Nature*,
   626(7999):549–554, 2024.
- 13. Avantika Gori and Ning Lin. Projecting compound flood hazard under climate change with physical models and joint probability methods. *Earth's Future*, 10(12):e2022EF003097, 2022.
- 14. Mahshid Ghanbari, Mazdak Arabi, Shih-Chieh Kao, Jayantha Obeysekera, and William
   Sweet. Climate change and changes in compound coastal-riverine flooding hazard
   along the US coasts. *Earth's Future*, 9(5):e2021EF002055, 2021.
- 15. Oliver EJ Wing, Paul D Bates, Andrew M Smith, Christopher C Sampson, Kris A Johnson, Joseph Fargione, and Philip Morefield. Estimates of present and future flood risk in the conterminous United States. *Environmental Research Letters*, 13(3):034023, 2018.
- 16. Ashish Sharma, Conrad Wasko, and Dennis P Lettenmaier. If precipitation extremes are increasing, why aren't floods? *Water resources research*, 54(11):8545–8551, 2018.

- 17. Danial Khojasteh, Steve Hottinger, Stefan Felder, Giovanni De Cesare, Valentin
  Heimhuber, David J Hanslow, and William Glamore. Estuarine tidal response to sea
  level rise: The significance of entrance restriction. *Estuarine, Coastal and Shelf Science*, 244:106941, 2020.
- 18. CL Lopes, MC Sousa, A Ribeiro, H Pereira, JP Pinheiro, L Vaz, and JM Dias. Evaluation of future estuarine floods in a sea level rise context, sci. rep., 12, 8083, 2022.
- 19. Charlotte Lyddon, Nguyen Chien, Grigorios Vasilopoulos, Michael Ridgill, Sogol Moradian, Agnieszka Olbert, Thomas Coulthard, Andrew Barkwith, and Peter Robins.

  Thresholds for estuarine compound flooding using a combined hydrodynamic—
  statistical modelling approach. *Natural Hazards and Earth System Sciences*,
  24(3):973–997, 2024.
- 20. Louise J Slater and Gabriele Villarini. Recent trends in US flood risk. *Geophysical Research Letters*, 43(24):12–428, 2016.
- 21. John Thomas Scharf and Thompson Westcott. *History of Philadelphia, 1609-1884*, volume 1. LH Everts & Company, 1884.
- 22. Schuylkill River Development Corporation. Improving stormwater management. https://www.schuylkillbanks.org/blog/
  improving-stormwater-management, 2018.
- Sebastian J Interlandi and Christopher S Crockett. Recent water quality trends in the
   schuylkill river, pennsylvania, usa: a preliminary assessment of the relative influences
   of climate, river discharge and suburban development. Water research, 37(8):1737–
   1748, 2003.

- <sup>528</sup> 24. Kerry Emanuel. Increasing destructiveness of tropical cyclones over the past 30 years.

  Nature, 436(7051):686–688, 2005.
- 25. Avantika Gori, Ning Lin, Dazhi Xi, and Kerry Emanuel. Tropical cyclone climatology change greatly exacerbates us extreme rainfall—surge hazard. *Nature Climate Change*, 12(2):171–178, 2022.
- 26. Karthik Balaguru, Wenwei Xu, Chuan-Chieh Chang, L Ruby Leung, David R Judi, Samson M Hagos, Michael F Wehner, James P Kossin, and Mingfang Ting. Increased us coastal hurricane risk under climate change. *Science advances*, 9(14):eadf0259, 2023.
- 27. Haijue Xu, Gang Wang, Zhe Huang, Yaqing Su, Yuchuan Bai, and Jiabo Zhang. Hydrodynamic interactions between tide and runoff in the luanhe estuary in bohai sea,
   china: From aquaculture reclamation to restoration. *Ocean & Coastal Management*,
   239:106586, 2023.
- 28. PM Orton, FEDERICO ROSARIO Conticello, Francesco Cioffi, TM Hall, N Georgas,
   Upmanu Lall, AF Blumberg, and K MacManus. Flood hazard assessment from storm
   tides, rain and sea level rise for a tidal river estuary. *Natural hazards*, 102:729–757,
   2020.
- Yawen Shen, Mohamed M Morsy, Chris Huxley, Navid Tahvildari, and Jonathan L
   Goodall. Flood risk assessment and increased resilience for coastal urban watersheds
   under the combined impact of storm tide and heavy rainfall. *Journal of Hydrology*,
   579:124159, 2019.
- 30. Jiun-Huei Jang and Tien-Hao Chang. Flood risk estimation under the compound influence of rainfall and tide. *Journal of Hydrology*, 606:127446, 2022.

- 31. Hamed R Moftakhari, Gianfausto Salvadori, Amir AghaKouchak, Brett F Sanders, and
  Richard A Matthew. Compounding effects of sea level rise and fluvial flooding. *Proceedings of the National Academy of Sciences*, 114(37):9785–9790, 2017.
- 32. Jin Teng, Anthony J Jakeman, Jai Vaze, Barry FW Croke, Dushmanta Dutta, and SJEM
   Kim. Flood inundation modelling: A review of methods, recent advances and uncertainty analysis. *Environmental modelling & software*, 90:201–216, 2017.
- 33. Paul Bates. Fundamental limits to flood inundation modelling. *Nature Water*, 1(7):566–
   567, 2023.
- 34. Vijendra Kumar, Kul Vaibhav Sharma, Tommaso Caloiero, Darshan J Mehta, and Karan
   Singh. Comprehensive overview of flood modeling approaches: A review of recent
   advances. *Hydrology*, 10(7):141, 2023.
- 35. Keighobad Jafarzadegan, Hamid Moradkhani, Florian Pappenberger, Hamed Moftakhari, Paul Bates, Peyman Abbaszadeh, Reza Marsooli, Celso Ferreira, Hannah L
   Cloke, Fred Ogden, et al. Recent advances and new frontiers in riverine and coastal flood modeling. *Reviews of Geophysics*, 61(2):e2022RG000788, 2023.
- 36. Sanaz Moghim, Mohammad Ahmadi Gharehtoragh, and Ammar Safaie. Performance
   of the flood models in different topographies. *Journal of Hydrology*, 620:129446, 2023.
- 567 37. Paul D Bates, Niall Quinn, Christopher Sampson, Andrew Smith, Oliver Wing, Jeison Sosa, James Savage, Gaia Olcese, Jeff Neal, Guy Schumann, et al. Combined modeling of us fluvial, pluvial, and coastal flood hazard under current and future climates.

  Water Resources Research, 57(2):e2020WR028673, 2021.
- 38. Adnan Rajib, Zhu Liu, Venkatesh Merwade, Ahmad A Tavakoly, and Michael L Follum.

- Towards a large-scale locally relevant flood inundation modeling framework using swat and lisflood-fp. *Journal of Hydrology*, 581:124406, 2020.
- 39. Iuliia Shustikova, Alessio Domeneghetti, Jeffrey C Neal, Paul Bates, and Attilio Castellarin. Comparing 2d capabilities of hec-ras and lisflood-fp on complex topography.

  Hydrological Sciences Journal, 64(14):1769–1782, 2019.
- 577 40. Xushu Wu, Zhaoli Wang, Shenglian Guo, Chengguang Lai, and Xiaohong Chen. A 578 simplified approach for flood modeling in urban environments. *Hydrology Research*, 579 49(6):1804–1816, 2018.
- 41. Beatriz Biguino, Ivan D Haigh, João Miguel Dias, and Ana C Brito. Climate change in
   estuarine systems: Patterns and gaps using a meta-analysis approach. Science of the
   Total Environment, 858:159742, 2023.
- David K. Li and Kathryn Prociv. Video shows destruction in Philadelphia area after

  Ida unleashes tornadoes, rain. https://www.nbcnews.com/news/weather/

  images-show-flooding-philadelphia-after-ida-unleashes-tornadoes-rain-n1

  2021. Accessed: 2021-09-02.
- 43. Billy Penn Staff. When Ida flooded the Vine Street Expressway a sight

  we hope to never see again. https://billypenn.com/2022/09/01/

  ida-flooding-philadelphia-vine-street-expressway-photos/,

  2021. Accessed: 2022-09-01.
- 44. Environmental Justice Office. Pennsylvania environmental justice mapping and screening tool (pennenviroscreen) methodology documentation 2023.

  https://files.dep.state.pa.us/PublicParticipation/Office%

- 20of%20Environmental%20Advocacy/EnvAdvocacyPortalFiles/2023/ 015-0501-003-InterimFinal.pdf, **2023**. Accessed: **2023-08-15**.
- <sup>596</sup> 45. Miyuki Hino and Earthea Nance. Five ways to ensure flood-risk research helps the most vulnerable. *Nature*, 595(7865):27–29, 2021.
- 46. Leonard O Ohenhen, Manoochehr Shirzaei, Chandrakanta Ojha, Sonam F Sherpa,
   and Robert J Nicholls. Disappearing cities on us coasts. *Nature*, 627(8002):108–115,
   2024.
- 47. Cheryl Tay, Eric O Lindsey, Shi Tong Chin, Jamie W McCaughey, David Bekaert,
   Michele Nguyen, Hook Hua, Gerald Manipon, Mohammed Karim, Benjamin P Horton,
   et al. Sea-level rise from land subsidence in major coastal cities. *Nature Sustainability*,
   5(12):1049–1057, 2022.
- 48. Leonard O Ohenhen, Guang Zhai, Jonathan Lucy, Susanna Werth, Grace Carlson,
   Mohammad Khorrami, Florence Onyike, Nitheshnirmal Sadhasivam, Ashutosh Tiwari,
   Khosro Ghobadi-Far, et al. Land subsidence risk to infrastructure in US metropolises.
   Nature Cities, 2025.
- 49. Anna Josephson and Maria I Marshall. The demand for post-Katrina disaster aid: SBA
   disaster loans and small businesses in Mississippi. *Journal of Contingencies and Crisis Management*, 24(4):264–274, 2016.
- 50. Benjamin L Collier, Sabrina T Howell, and Lea Rendell. After the storm: How emergency liquidity helps small businesses following natural disasters. Technical report,
   National Bureau of Economic Research, 2024.
- 51. Aswath Damodaran. *Investment valuation: Tools and techniques for determining the*value of any asset. John Wiley & Sons, 2012.

- 52. Ben Strauss, Claudia Tebaldi, and Scott Kulp. Pennsylvania and the Surging Sea. https://sealevel.climatecentral.org/research/reports/
   pennsylvania-and-the-surging-sea, 2016.
- 53. Andra J Garner, Michael E Mann, Kerry A Emanuel, Robert E Kopp, Ning Lin, Richard B
   Alley, Benjamin P Horton, Robert M DeConto, Jeffrey P Donnelly, and David Pollard.
   Impact of climate change on New York City's coastal flood hazard: Increasing flood
   heights from the preindustrial to 2300 CE. *Proceedings of the National Academy of Sciences*, 114(45):11861–11866, 2017.
- 54. Paul Bates. Uneven burden of urban flooding. *Nature Sustainability*, 6(1):9–10, 2023.
- 55. Martin Hoerling, Jon Eischeid, Judith Perlwitz, Xiao-Wei Quan, Klaus Wolter, and Linyin
   Cheng. Characterizing recent trends in US heavy precipitation. *Journal of Climate*,
   29(7):2313–2332, 2016.
- 56. Paul CD Milly, Julio Betancourt, Malin Falkenmark, Robert M Hirsch, Zbigniew W
   Kundzewicz, Dennis P Lettenmaier, and Ronald J Stouffer. Stationarity is dead:
   Whither water management? Science, 319(5863):573–574, 2008.
- 57. Mohammad Kazem Sharifian, Georges Kesserwani, Alovya Ahmed Chowdhury, Jef frey Neal, and Paul Bates. Lisflood-fp 8.1: new gpu-accelerated solvers for faster
   fluvial/pluvial flood simulations. *Geoscientific Model Development*, 16(9):2391–2413,
   2023.
- 58. Kaighin A McColl. Practical and theoretical benefits of an alternative to the penman-monteith evapotranspiration equation. Water Resources Research, 56(6):e2020WR027106, 2020.

- 59. Alice K Li, Yue Mao, Sandeep Manjanna, Sixuan Liu, Jasleen Dhanoa, Bharg Mehta,
   Victoria M Edwards, Fernando Cladera Ojeda, M Ani Hsieh, Maël Le Men, et al. To wards understanding underwater weather events in rivers using autonomous surface
   vehicles. In OCEANS 2022, Hampton Roads, pages 1–8. IEEE, 2022.
- 60. Louise J Slater, Michael Bliss Singer, and James W Kirchner. Hydrologic versus geo morphic drivers of trends in flood hazard. *Geophysical Research Letters*, 42(2):370–
   376, 2015.
- 646 61. Andrea J Linscott. Natural disasters—a microbe's paradise. *Clinical Microbiology*647 *Newsletter*, 29(8):57–62, 2007.
- 648 62. John T Watson, Michelle Gayer, and Maire A Connolly. Epidemics after natural disas-649 ters. *Emerging infectious diseases*, 13(1):1, 2007.
- 650 63. UC Nkwunonwo, M Whitworth, and B Baily. A review of the current status of flood mod-651 elling for urban flood risk management in the developing countries. *Scientific African*, 652 7:e00269, 2020.
- 64. Mahmut Tudaji, Yi Nan, and Fuqiang Tian. Assessing the value of high-resolution rainfall and streamflow data for hydrological modeling: an analysis based on 63 catchments in southeast China. *Hydrology and Earth System Sciences*, 29(7):1919–1937, 2025.
- 656 65. Jochen Hinkel, Daniel Lincke, Athanasios T Vafeidis, Mahé Perrette, Robert James
   Nicholls, Richard SJ Tol, Ben Marzeion, Xavier Fettweis, Cezar Ionescu, and Anders
   Levermann. Coastal flood damage and adaptation costs under 21st century sea-level
   rise. Proceedings of the National Academy of Sciences, 111(9):3292–3297, 2014.
- 66. Michelle A Hummel, Robert Griffin, Katie Arkema, and Anne D Guerry. Economic

- evaluation of sea-level rise adaptation strongly influenced by hydrodynamic feedbacks. *Proceedings of the National Academy of Sciences*, 118(29):e2025961118, 2021.
- 663 67. Jonathan WF Remo, Megan Carlson, and Nicholas Pinter. Hydraulic and flood-loss 664 modeling of levee, floodplain, and river management strategies, middle mississippi 665 river, usa. *Natural hazards*, 61:551–575, 2012.
- 666 68. Brenden Jongman. Effective adaptation to rising flood risk. *Nature communications*, 9(1):1986, 2018.
- 69. Shiqiang Du, Paolo Scussolini, Philip J Ward, Min Zhang, Jiahong Wen, Luyang Wang,
   Elco Koks, Andres Diaz-Loaiza, Jun Gao, Qian Ke, et al. Hard or soft flood adapta tion? Advantages of a hybrid strategy for Shanghai. *Global Environmental Change*,
   61:102037, 2020.
- 70. Vincent TM van Zelst, Jasper T Dijkstra, Bregje K van Wesenbeeck, Dirk Eilander, Edward P Morris, Hessel C Winsemius, Philip J Ward, and Mindert B de Vries. Cutting the costs of coastal protection by integrating vegetation in flood defences. *Nature* communications, 12(1):6533, 2021.
- 71. Leanne Archer, Jeffrey Neal, Paul Bates, Emily Vosper, Dereka Carroll, Jeison Sosa, and Daniel Mitchell. Current and future rainfall-driven flood risk from hurricanes in puerto rico under 1.5°c and 2°c climate change. *EGUsphere*, 2023:1–32, 2023.
- 72. Simbidzayi Hatchard, Rafael JP Schmitt, Francesca Pianosi, James Savage, and Paul
  Bates. Strategic siting and design of dams minimizes impacts on seasonal floodplain
  inundation. *Environmental Research Letters*, 2023.
- 73. Mohamed Soliman, Mohamed M Morsy, and Hany G Radwan. Assessment of imple-

- menting land use/land cover lulc 2020-esri global maps in 2d flood modeling application. *Water*, 14(23):3963, 2022.
- 74. Narayan Nyaupane. *Statistical Evaluation of Hydrological Extremes on Stormwater*Systems. Southern Illinois University at Carbondale, 2018.
- 75. Cristian Martinez-Villalobos and J David Neelin. Why do precipitation intensities tend to follow gamma distributions? *Journal of the Atmospheric Sciences*, 76(11):3611–3631, 2019.
- 76. Wiesław Gądek, Beata Baziak, Tamara Tokarczyk, and Wiwiana Szalińska. A novel
   method of design flood hydrographs estimation for flood hazard mapping. Water,
   14(12):1856, 2022.
- 77. Monomoy Goswami. Generating design flood hydrographs by parameterizing the characteristic flood hydrograph at a site using only flow data. *Hydrological Sciences Journal*, 67(16):2505–2523, 2022.
- 78. Jacob T VanderPlas. Understanding the lomb–scargle periodogram. *The Astrophysical Journal Supplement Series*, 236(1):16, 2018.
- 79. Xiucheng Yang, Qiming Qin, Pierre Grussenmeyer, and Mathieu Koehl. Urban surface water body detection with suppressed built-up noise based on water indices from sentinel-2 msi imagery. *Remote sensing of environment*, 219:259–270, 2018.
- 80. Oliver EJ Wing, Paul D Bates, Christopher C Sampson, Andrew M Smith, Kris A Johnson, and Tyler A Erickson. Validation of a 30 m resolution flood hazard model of the
   conterminous u nited s tates. Water Resources Research, 53(9):7968–7986, 2017.
- <sub>704</sub> 81. Cort J Willmott. On the validation of models. *Physical geography*, 2(2):184–194, 1981.

82. Dingyu Xuan and Hugo N. Ulloa. Compound flood modelling in the philadelphia schuylkill system, October 2025.